

# Nonlinear signal-processing model for scalar diffraction in optical recording

Wim M. J. Coene

A nonlinear signal-processing model is derived for the optical recording channel based on scalar diffraction theory. In this model, the signal waveform is written in closed form as an explicit function of the channel bits that are stored on an optical disk, thereby comprising both linear and nonlinear terms. Its explicit dependence on the channel bits makes this model well suited for signal-processing purposes. With the model it is also convenient to assess the importance of nonlinear contributions to the signal waveform. The model is applied for one-dimensional optical storage as well as for two-dimensional (2D) optical storage in which bits are arranged on a 2D hexagonal lattice. Signal folding is addressed as a typical nonlinear issue in 2D optical storage and can be eliminated by recording of pit marks of sizes considerably smaller than the size of the hexagonal bit cell. Further simplifications of the model with only a limited number of channel parameters are also derived. © 2003 Optical Society of America

OCIS codes: 210.0210, 210.4590, 210.4770, 260.1960.

## 1. Introduction

Accurate simulation of signal waveforms as obtained during readout of optical disks is important, for instance, for the design of new optical recording formats. A completely rigorous approach would necessitate inclusion of vector diffraction effects,<sup>1,2</sup> but doing so would be impractical because of computational complexity. A more convenient and still sufficiently accurate way of simulation is accomplished with a model based on scalar diffraction theory as introduced by Hopkins.<sup>3</sup> The scalar diffraction model considers the complex-valued optical wave front of the scanning laser spot, denoted  $p(\mathbf{R} - \mathbf{R}_p)$ , that is incident at a position  $\mathbf{R}_p$  in the two-dimensional (2D) plane of the information layer on the disk ( $\mathbf{R}$  is the 2D position vector in that plane); the optical wave front is subsequently diffracted by the marks (or pits) and nonmarks (or lands) on the disk, after which it propagates back through the objective lens toward the photodetector. The information layer is represented by a (complex-valued) reflection function, denoted  $r(\mathbf{R})$ . For the commonly used central-aperture detection (CA), the power of

the optical wave front is integrated within the detection aperture, which is located in the exit pupil of the objective lens: This yields the signal waveform, which is denoted  $I(\mathbf{R}_p)$  (with the laser spot at position  $\mathbf{R}_p$  in the plane of the disk), for which one has

$$I(\mathbf{R}_p) = \int_{(CA)} |\text{FT}_{\mathbf{R} \rightarrow \Omega}[p(\mathbf{R} - \mathbf{R}_p)r(\mathbf{R})]|^2 d\Omega, \quad (1)$$

where  $\Omega$  represents the 2D spatial frequency vector in the plane of the exit pupil of the objective lens and FT denotes a 2D Fourier transform from the disk's plane ( $\mathbf{R}$ ) toward the plane of the exit pupil ( $\Omega$ ).

Inasmuch as the terminology used in Hopkins's formalism comprises optical wavefronts, 2D Fourier transforms, and disk-reflection functions, it is not of direct use for signal-processing purposes for which one aims for a closed-form expression of the signal waveform in terms of the channel bits that are written to the disk. Such an explicit form in terms of the channel bits is required, for instance, for evaluation of the nonlinearities in the signal waveform: After a proper understanding of their origin is obtained, these nonlinearities can be combatted efficiently in the bit-detection module of the digital receiver by use of proper signal-processing measures. A commonly used approach that circumvents the drawback described above is to consider only instances of linear interference in the optical storage channel, thereby assuming that the linear are much more important

Wim M. J. Coene (wim.coene@philips.com) is with Philips Research Laboratories, Prof. Holstlaan 4 (WY31), 5656 AA Eindhoven, The Netherlands.

Received 11 April 2003.

0003-6935/03/326525-11\$15.00/0

© 2003 Optical Society of America

than the nonlinear contributions. Note the intrinsic nonlinear character of the signal waveform in Eq. (1), as it results from detection of the power of the optical wave front at the photodetector. In the linear approximation, bit-synchronous signal waveform  $I_k$  (at bit position  $k$ ) is obtained as the convolution of the bipolar channel bit sequence  $b_k$  (with values  $\pm 1$ ) and the impulse-response function (IRF) [also known as the point-spread function (PSF)] of the channel, denoted  $h_k$ , that is,

$$I_k = \sum_n h_{k-n} b_n. \quad (2)$$

Impulse response function  $h_k$  is computed as the FT of the modulation transfer function, denoted  $H(\Omega)$ , which is given by a formula known in the optical storage signal-processing community as the Braat–Hopkins formula<sup>4</sup> (see also Chap. 6 of Ref. 5):

$$H(\Omega) = \frac{2}{\pi} \left\{ \begin{array}{l} \arccos\left(\frac{\Omega}{\Omega_c}\right) \\ - \frac{\Omega}{\Omega_c} \left[ 1 - \left(\frac{\Omega}{\Omega_c}\right)^2 \right]^{1/2} \end{array} \right\} \quad \Omega \leq \Omega_c \\ = 0 \quad \Omega > \Omega_c. \quad (3)$$

In Eq. (3) the cutoff frequency of the channel beyond which no information is transferred is denoted  $\Omega_c$  and is defined as

$$\Omega_c = 2NA/\lambda, \quad (4)$$

where  $\lambda$  is the wavelength of the light and NA is the numerical aperture of the objective lens.

Obviously, the linear approach that uses the Braat–Hopkins formula, although it is elegant from a signal-processing point of view, is—by definition—not capable of coping with nonlinear effects such as pit–land asymmetry. That nonlinear effect is prominent in conventional optical recording media such as CDs and DVDs: It can almost directly be observed from many eye patterns as the (mostly) downward shift of the inner eye (the inner eye originates from the shortest run lengths of the run-length-limited code used) relative to the (minimum and maximum) signal levels that correspond to the longest run lengths (see Ref. 6 for more details). Recently Kobayashi<sup>7</sup> introduced an improved and elegant method that can handle the nonlinearities with a high level of accuracy, with the additional advantage that it is directly suited for signal-processing purposes: The nonlinear terms are computed as the convolution between a so-called edge-spread function (ESF) and a series of  $\delta$  impulses that are located at the transitions in the channel bit stream (the transitions occur from a pit run to a land run and vice versa). The shapes of the ESF and the PSF turn out to be almost identical. This observation explains why the so-called A-parameter model<sup>8</sup> for pit–land asymmetry, which is a phenomenological model (somewhat related to the ESF model<sup>7</sup>), works well to describe the experimental signal waveforms. The A-parameter model

transforms a fraction of the bipolar bits of a given polarity (either +1 or –1), namely, those that are neighbors of the transitions in the channel bit stream, into a nonbinary value; after the binary bit stream is replaced by the ternary bit stream (they differ only at transitions), the bit stream is convolved with the standard PSF [just as in Eq. (2)]. An alternative approach<sup>9</sup> that handles nonlinear effects in optical recording decomposes the optical wave front into a number of separate components that are based on the various tracks within the area of the illuminating spot. A related decomposition in yet another approach<sup>10</sup> is based on contributions from individual marks. Both approaches<sup>9,10</sup> stress the importance of the nonlinear effects; however, unlike in the ESF model<sup>7</sup> and the A-parameter model,<sup>8</sup> they are not directly suited for signal-processing purposes.

A new concept for 2D optical storage is being developed in which the channel bits are arranged on a 2D hexagonal lattice. A characteristic feature of 2D optical storage is that the distance of a bit to its neighboring bits is identical for all (tangential and radial) directions, much unlike the situation in one-dimensional (1D) optical storage for which the radial distances are significantly larger, leaving a considerable land portion between successive tracks. Because of this feature, signal nonlinearities in 2D optical storage are expected to be much more prominent. Furthermore, in 2D optical storage the concept of contiguous pit marks, as it applies for the 1D case, needs to be abandoned to reduce the nonlinearities. Altogether, 2D extensions of the previously mentioned models (ESF model and A-parameter model) for conventional 1D optical storage are not appropriate for describing the nonlinearities for 2D optical storage; consequently a new signal-processing model (based on scalar diffraction) needs to be designed. The derivation of this new signal-processing model is the main topic of this paper. The model is generic in the sense that it can be applied to conventional 1D optical recording as well, as an alternative to the ESF model. Unlike most of the methods mentioned above, the signal-processing model described in this paper does not require any additional approximation: It is completely identical to Hopkins's scalar diffraction approach. Apart from linear intersymbol interference (ISI), which is described by (an adapted form of) the IRF or the PSF, the model also includes a separate nonlinear kernel for the nonlinear ISI.

The outline of this paper is as follows: In Section 2 the new signal-processing model is introduced as the central topic of the paper. Its application to 1D optical storage is described in Section 3. Section 4 deals with application to 2D optical storage. For 2D optical storage with a rotationally symmetric laser spot, a simplified signal-processing model with a reduced number of channel parameters is derived in Section 5. Options for future related research are addressed in the concluding Section 6.

## 2. Nonlinear Signal-Processing Model

The derivation of the model is based on two steps: First we need a convenient representation of the disk reflection function  $r(\mathbf{R})$  as a function of the channel bits that are written to the disk; second, in Eq. (1) the order of integration over the central aperture and the summation over bits [which results from the expression for  $r(\mathbf{R})$ ] is interchanged. We first introduce a number of definitions. On the information layer of the disk we identify pit areas, which have a reflection function equal to  $\exp(i\phi)$ , where  $\phi$  is the double-pass phase depth, and land areas, which have a reflection function equal to 1. With a pit bit ( $b_j = +1$ ), we associate a pit area defined by the pit window function  $W(\mathbf{R} - \mathbf{R}_j)$  centered at bit position  $\mathbf{R}_j$ : We have that  $W = 1$  inside the pit area and  $W = 0$  outside the pit area. Consequently a land bit ( $b_j = -1$ ) is characterized by the absence of such a pit area. In this model, pit window functions of neighboring pit bits are assumed to be nonoverlapping.

Disk reflection function  $r(\mathbf{R})$  can then be written in the following notation:

$$r(\mathbf{R}) = 1 + \sum_j a_j W(\mathbf{R} - \mathbf{R}_j). \quad (5)$$

In Eq. (5),  $a_j$  represents the complex-valued bit value for the bit at position  $\mathbf{R}_j$ , which accounts for the difference in reflection between a land area and a pit area. With  $u_j$  denoting the unipolar bit values (0, 1) derived from the bipolar bit values ( $\pm 1$ ) by

$$u_j = \frac{1 + b_j}{2}, \quad (6)$$

bit parameter  $a_j$  is defined as

$$a_j = u_j [\exp(i\phi) - 1]. \quad (7)$$

Note that disk reflection function  $r(\mathbf{R})$  of Eq. (5) explicitly reflects the asymmetry between land and pit bits: For land bits we have that  $a_j = 0$ , so the area occupied by a land bit is physically identical to the so-called virginial disk (without any pit bits).

For notational convenience we introduce the so-called bracket notation for the complex-valued optical wave front in the plane of the exit pupil. The bracket notation is well known in quantum mechanics, where it was introduced by Dirac<sup>11</sup>: it allows interference integrals of the type used in Eq. (1) to be written in extremely compact form. Accordingly, we rewrite the complex-valued optical wave function in the exit pupil as

$$|\psi\rangle = \text{FT}_{\mathbf{R} \rightarrow \Omega} [p(\mathbf{R} - \mathbf{R}_p) r(\mathbf{R})]. \quad (8)$$

The inner product (or bracket) of two functions, the bra  $\langle\phi|$  and the ket  $|\varphi\rangle$ , is defined by the integral within the CA used for detection:

$$\langle\phi|\varphi\rangle = \int_{(\text{CA})} \phi^*(\Omega) \varphi(\Omega) d\Omega. \quad (9)$$

Hence the detected signal waveform according to Hopkins's scalar diffraction model becomes simply

$$I = \langle\psi|\psi\rangle. \quad (10)$$

Combining Eqs. (5) and (8) yields

$$|\psi\rangle = |\psi_L\rangle + \sum_j a_j |\psi_j\rangle. \quad (11)$$

Equation (11) represents a decomposition of  $|\psi\rangle$  into a number of terms. The first term is the wave front for the all-land situation when the optical disk contains only land bits (no pit marks), that is, when the disk surface is a perfect mirror; it is denoted  $|\psi_L\rangle$  and is given by

$$|\psi_L\rangle = \text{FT}_{\mathbf{R} \rightarrow \Omega} [p(\mathbf{R} - \mathbf{R}_p)]. \quad (12)$$

The second term in Eq. (11) is a sum of contributions to the pupil wave front from all individual pit bits that are present in the information layer within the effective range of the spot. Each contribution of the second term contains a wave function  $|\psi_j\rangle$  (called briefly the "pit wave front") for a pit mark at position  $\mathbf{R}_j$ , which is given by

$$|\psi_j\rangle = \text{FT}_{\mathbf{R} \rightarrow \Omega} [p(\mathbf{R} - \mathbf{R}_p) W(\mathbf{R} - \mathbf{R}_j)]. \quad (13)$$

Using Eq. (11) in Eq. (10) finally yields the signal waveform as

$$I = \langle\psi_L|\psi_L\rangle + \sum_j a_j \langle\psi_L|\psi_j\rangle + \sum_j a_j^* \langle\psi_j|\psi_L\rangle + \sum_{j,k} a_k^* a_j \langle\psi_k|\psi_j\rangle. \quad (14)$$

Equation (14) is the basic formula of this paper. Signal waveform  $I$  of Eq. (14) is nonlinearly dependent on channel bits  $b_j$  through complex-valued coefficients  $a_j$ . The first term in Eq. (14) is a constant term, reflecting the maximum amplitude of the signal that occurs when there are no pits on the disk: It is the self-interference of all-land wave front  $|\psi_L\rangle$ . The next two terms in Eq. (14) represent that part of the signal that is linearly dependent on channel bits  $u_j$ : These terms are due to linear interference between all-land wave front  $|\psi_L\rangle$  and pit wave front  $|\psi_j\rangle$ . The last term in Eq. (14) is the bilinear term, which corresponds to the interference between the wave fronts that results from two pit bits, at positions  $\mathbf{R}_j$  and  $\mathbf{R}_k$ , that contribute to the signal waveform with the laser spot focused at  $\mathbf{R}_p$ .

We derive from Eq. (14) an expression that is directly suitable from a signal-processing point of view. First, for the sake of simplicity, we normalize all terms by a common gain factor such that the land-land interference term  $\langle\psi_L|\psi_L\rangle$ , which is the maximum level of the signal waveform, equals 1 (for this situation the disk's surface is a perfect mirror). Sec-

ond, we make use of the following properties of the kernels for linear and nonlinear interferences:

$$\langle \psi_L | \psi_j \rangle = \langle \psi_j | \psi_L \rangle = \int |p(\mathbf{R} - \mathbf{R}_p)|^2 W(\mathbf{R} - \mathbf{R}_j) d\mathbf{R} \in \mathcal{R}, \quad (15)$$

$$\langle \psi_j | \psi_k \rangle = \langle \psi_k | \psi_j \rangle^*. \quad (16)$$

The integral in Eq. (15) was obtained by application of Parseval's theorem and from the fact that  $|\psi_L\rangle$  is band limited within the central aperture. Equation (15) reveals an elegant physical interpretation of the coefficients for linear interference: They are just the integral of the power of the laser spot  $|p|^2$  computed within pit window  $W$  for the pit bit considered at a certain position ( $\mathbf{R}_j$ ) relative to the center of the spot ( $\mathbf{R}_p$ ). Third, for unipolar bit value  $u_j$  (0, 1) we have that  $u_i^2 = u_i$ . Finally, we can rewrite Eq. (14) in compact form as

$$I = 1 - \sum_j c_j u_j + \sum_{j \neq k} e_{j,k} u_j u_k, \quad (17)$$

where the coefficients  $c_j$  for the linear ISI are given by

$$c_j = 2[1 - \cos(\phi)](\langle \psi_L | \psi_j \rangle - \langle \psi_j | \psi_j \rangle) \quad (18)$$

and where the coefficients  $e_{j,k}$  for nonlinear ISI are given by

$$e_{j,k} = 2[1 - \cos(\phi)]\text{Re}(\langle \psi_j | \psi_k \rangle). \quad (19)$$

The coefficients for the linear ISI,  $c_j$ , are a combination of the (linear) interference term between the all-land wave front and a pit wave front  $\langle \psi_L | \psi_j \rangle$  and of the (nonlinear) self-interference term  $\langle \psi_j | \psi_j \rangle$  for a pit wave front. Note that we reserve the term “interference” to be used for optical wave fronts as in Eq. (14), whereas we adhere to the term intersymbol interference for interference of bits, as in Eq. (17).

Another observation from Eqs. (18) and (19) is that the geometry of a pit bit (determined by pit window  $W$ ) and phase depth  $\phi$  of a pit bit are decoupled. The factor related to the phase depth is identical for both sets of coefficients and equals  $2[1 - \cos(\phi)]$ . Consequently, a change in the phase depth of the pit marks will affect only the modulation range (minimum and maximum signal levels) of the signal waveform but not its overall shape.

A practical simulation based on Eq. (14) or Eq. (17) is performed in two steps as follows: In a first step, all the relevant linear and nonlinear coefficients ( $\langle \psi_L | \psi_j \rangle$  and  $\langle \psi_k | \psi_j \rangle$ ), or, equivalently,  $c_j$  and  $e_{j,k}$  are precomputed (e.g., by use of fast FTs) for the conditions of the optical channel at hand ( $\lambda$ , NA, and track and pit geometries). In a second step, the signal waveform for a given channel bit stream  $b_j$  is computed according to Eq. (14) or Eq. (17).

Equation (17) holds for any arbitrary sampling phase of the laser spot; that is, position  $\mathbf{R}_p$  of the laser spot can be at any possible location in the 2D plane of the disk. However, linear and nonlinear kernels  $c_i$  and  $e_{i,j}$  depend on the actual sampling phase; thus,

for each sampling phase that is required in a given simulation, a separate pair of kernels ( $c_i$  and  $e_{i,j}$ ) has to be precomputed.

We conclude this section with a remark on the expansion for disk reflection function  $r(\mathbf{R})$  in Eq. (5). It has been implicitly assumed that the pit window  $W$  has infinitely steep vertical edges: This assumption resulted in a separate factor for phase depth  $\phi$ . For a more realistic situation in which pit bits are represented by a pit area that has edges of a limited steepness, the above formalism needs to be modified slightly. Let window  $W$  still represent the area of the pit outside of which we have that  $r(\mathbf{R}) = 1$ . We then need to replace the constant phase depth  $\phi$ , assumed in the analysis above, by a position-dependent phase depth, denoted  $\phi(\mathbf{R} - \mathbf{R}_j)$ . In that case the previous analysis with linear and nonlinear kernels remains valid after disk reflection function  $r(\mathbf{R})$  is rewritten as

$$r(\mathbf{R}) = 1 + \sum_j u_j \tilde{W}_\phi(\mathbf{R} - \mathbf{R}_j),$$

with, for the complex-valued modified window function  $\tilde{W}_\phi$ ,

$$\tilde{W}_\phi(\mathbf{R} - \mathbf{R}_j) = \{\exp[i\phi(\mathbf{R} - \mathbf{R}_j)] - 1\}W(\mathbf{R} - \mathbf{R}_j).$$

Obviously the most important difference from the previous analysis is that the integrals for computation of the resultant linear and nonlinear kernels should in this case include position-dependent phase depths  $\phi(\mathbf{R} - \mathbf{R}_j)$ . Note that, for the applications described henceforth, we assume infinitely steep edges.

### 3. Application to One-Dimensional Optical Storage

The model of Section 2 was applied to a DVD-ROM system with the following physical parameters:  $\lambda = 650$  nm; NA = 0.60; channel bit length,  $T = 133$  nm; radial pit width, 260 nm. The linear interference kernels  $\langle \psi_L | \psi_j \rangle$  are shown in Fig. 1; the nonlinear interference kernels  $\langle \psi_k | \psi_j \rangle$  are shown in Fig. 2 for several values of bit position  $j$  (note that the prefactor that is due to phase depth  $\phi$  of the pits is not included). The typical shapes of the curves for the nonlinear kernels are illustrated in Fig. 2: They are reminiscent of the shape of the spot profile, and the tap values depend on the actual locations of interfering bits  $j$  and  $k$  within the spot profile. Therefore the tap with the maximum value shifts with the position of bit  $j$ , and its magnitude decreases with increasing  $j$ . For  $\phi = 180^\circ$ , Fig. 3 shows the simulated signal waveform for a typical bit sequence: The complete signal is shown, together with its linear approximation (with constant term 1 and the linear contributions that are due to  $\langle \psi_L | \psi_j \rangle$ ) and with the separate nonlinear contributions related to  $\langle \psi_k | \psi_j \rangle$  for different values of  $|k - j|$ . From Fig. 3 we can observe that the nonlinear contributions are very small in the center area of long land runs ( $5T$  and  $11T$ ) but are nonnegligible at the center of the shortest land runs which are equal to  $3T$ ; also, at the edge regions of the long

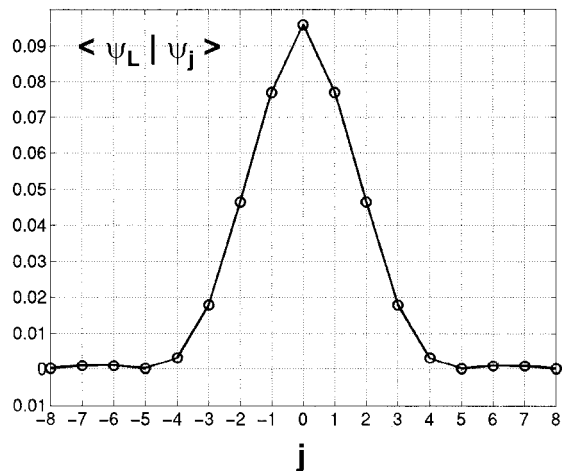


Fig. 1. Coefficients for linear interference kernels  $\langle \psi_L | \psi_j \rangle$  for a DVD pick-up unit ( $\lambda = 650$  nm; NA = 0.60). Channel bit length  $T = 133$  nm; radial pit width, 260 nm. The laser spot is centered at bit position  $j = 0$ .

land runs there are some nonlinear contributions from the pit bits in the neighboring pit runs. The nonlinear contributions are most significant in the center area of long pit runs, and their amplitude increases with increasing run length. The next-neighbor nonlinearity that is due to  $\langle \psi_{j \pm 1} | \psi_j \rangle$  is the most important one, but the other contributions with values of  $|k - j|$  of as much as 4 are not negligible. For the DVD conditions considered, the resultant eye pattern is drawn in Fig. 4: An eye pattern consists of many overlaid traces of small sections of the signal waveform, all synchronized to the bit clock. In Fig. 4 a pit-land asymmetry of  $\sim 16\%$  is clearly observable.

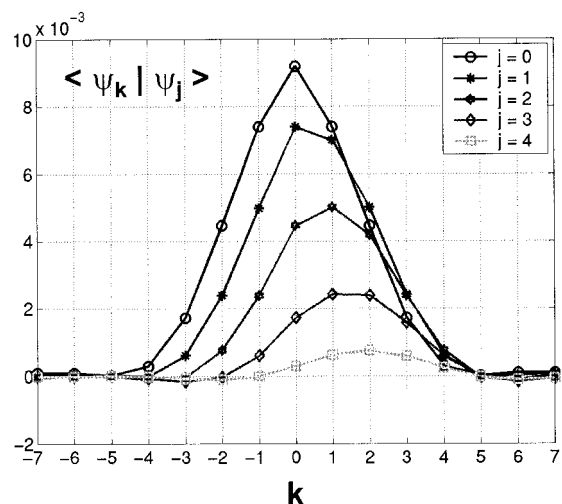


Fig. 2. Coefficients for nonlinear interference kernels  $\langle \psi_k | \psi_j \rangle$  for a DVD pick-up unit ( $\lambda = 650$  nm; NA = 0.60). Channel bit length,  $T = 133$  nm; radial pit width, 260 nm. The laser spot is centered at bit position  $j = 0$ .

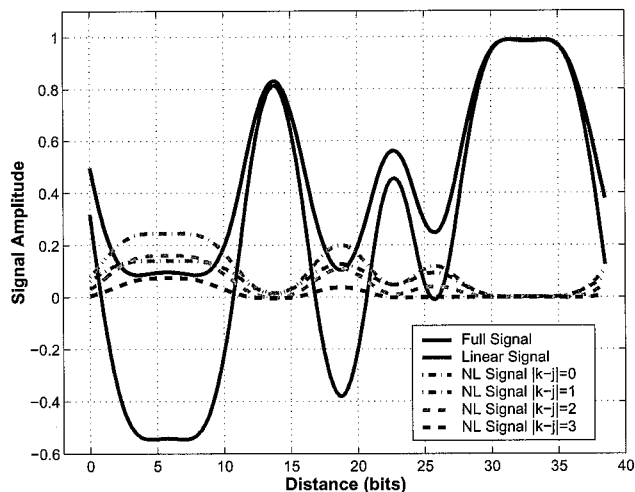


Fig. 3. Simulated signal waveform according to the model of Section 2 for a DVD pick-up unit ( $\lambda = 650$  nm; NA = 0.60). Channel bit length,  $T = 133$  nm; radial pit width, 260 nm. The channel bit sequence is  $-11T-5T-5T-3T-3T-11T$ . The complete signal waveform, the linear approximation (with constant term 1 and the linear contributions with  $\langle \psi_L | \psi_j \rangle$ ), and the separate nonlinear (NL) contributions related to  $\langle \psi_k | \psi_j \rangle$ , where  $|k - j| = 0, 1, 2$  and 3, are shown.

#### 4. Application to Two-Dimensional Optical Storage

A new concept for 2D optical storage is currently being developed in which the information on the disk fundamentally has a 2D character.<sup>12,13</sup> The aim is to achieve an increase over the third generation of optical storage [Blu-ray Disc (BD) with wavelength  $\lambda = 405$  nm and a NA of 0.85; see Refs. 14 and 15] by a factor of 2 in data density and by a factor of 10 in data rate (for the same physical parameters of the optical readout system). In this new concept, the bits are organized in a broad spiral. Such a spiral consists of a number of bit rows stacked one upon another with a fixed phase relation in the radial direction, such that the bits are arranged on a 2D lattice. A 2D closed-packed hexagonal ordering of the bits is chosen because it has a 15% higher packing

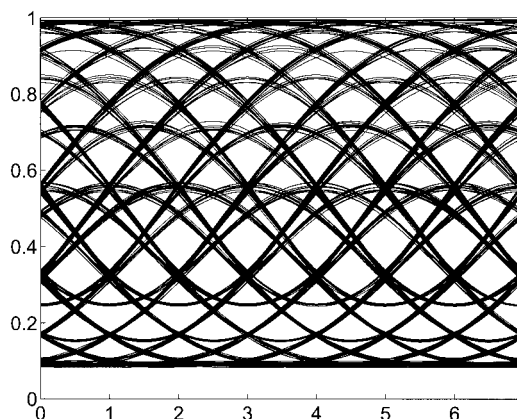


Fig. 4. Simulated eye pattern according to the model of Section 2 for a DVD pick-up unit ( $\lambda = 650$  nm; NA = 0.60). Channel bit length,  $T = 133$  nm; radial pit width, 260 nm.

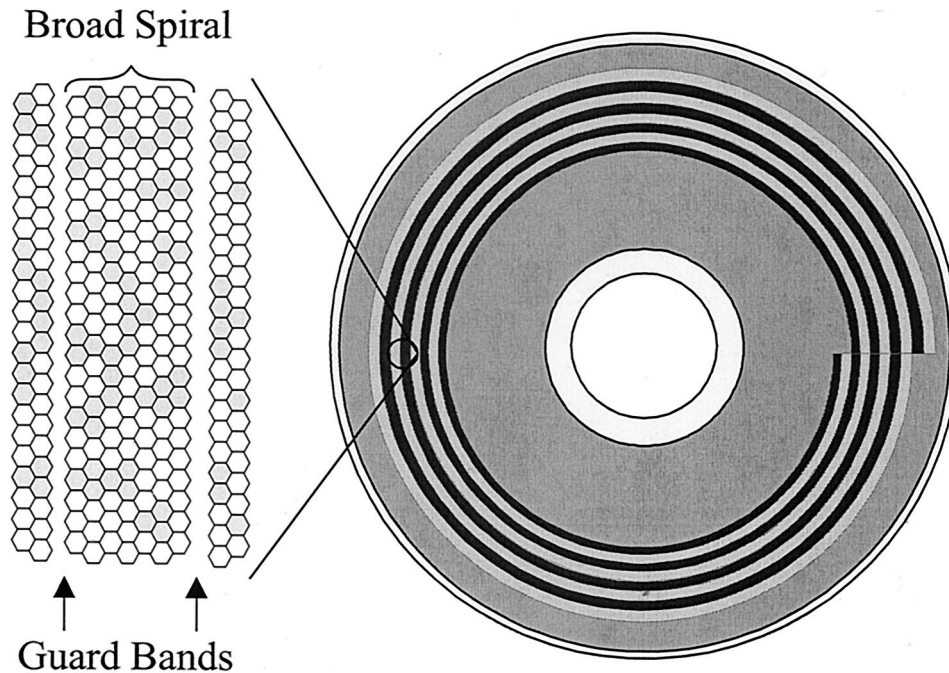


Fig. 5. Schematic format for 2D optical storage (for simplicity, a seven-row broad spiral is shown). Each hexagon corresponds to a bit cell (white for bit 0, gray for bit 1).

fraction than the square lattice.<sup>16,17</sup> Successive revolutions of the broad spiral are separated by a guard band consisting of one empty bit row (Fig. 5). A multispot light path for parallel readout is realized, where each spot has BD characteristics. Signal processing with equalization, timing recovery, and bit detection is carried out in a 2D fashion, that is, jointly over all the bit rows within the broad spiral.<sup>12,13</sup>

For 1D optical storage with a small pit-land asymmetry, the linear model of Eq. (2) is quite a reasonable approximation for the channel, irrespective of whether we use the Braat-Hopkins IRF of Eq. (3) or the IRF from Kobayashi.<sup>7</sup> In such a linear model, long land runs and long pit runs lead to maximum and minimum signal amplitudes, respectively. The reason why a long pit mark has a small signal amplitude is that the spot diameter is normally larger than the radial width of a pit on the disk. Hence, when the spot scans such a long pit mark, the reflected light beam loses intensity merely by radial diffraction outside the CA of the lens. Note that Kobayashi's<sup>7</sup> linear IRF indeed takes account of the finite radial extent of a pit, whereas the Braat-Hopkins IRF is based on purely tangential diffraction from phase fronts that vary sinusoidally in the tangential direction but are constant in the radial direction; nevertheless, despite this basic conceptual difference, the two approaches yield quite similar impulse responses. For 2D optical storage, however, nonlinear effects are substantially more important, as is explained in the remainder of this section.

A characteristic feature of 2D optical storage is that the distance of a bit to its neighboring bits is identical for all (tangential and radial) directions,

quite unlike the situation for 1D optical storage for which the radial distances are significantly larger, leaving a considerable land portion between successive tracks. This intermediate land portion is missing in the 2D case: Therefore the problem of what we may call signal folding may arise when the pit mark for a pit bit is assumed to cover the complete hexagonal bit cell. For a large contiguous pit area consisting of a number of neighboring pit bits, there is no diffraction at all: Consequently, a large pit area and a large nonpit (or land) area will show identical readout signals because they both act as perfect mirrors. As a result the channel becomes highly nonlinear. In view of robust bit detection in 2D optical storage, the signal waveform should preferably show a systematic roll-off (which should be as linear as possible) for an increasing number of neighboring bits of the pit type: This property must hold for both possible bit values for the central bit. Signal folding occurs when the central bit is of the pit type, that is, a 1 bit: (Part of) the signal values increase (instead of decrease) with an increasing number of neighboring pit bits. One can eliminate signal folding by recording each pit bit as a separate pit hole with a size considerably smaller than the size of the hexagonal bit cell. In this way, large contiguous areas of pit marks are prevented because the pit holes are always separated by intermediate land areas, leading to diffraction outside the CA.

We now quantify the nonlinearities of the 2D optical storage channel in more detail. With the nonlinear signal-processing model for scalar diffraction as outlined in Section 2, the signal levels for all possible hexagonal clusters are calculated. A hex-

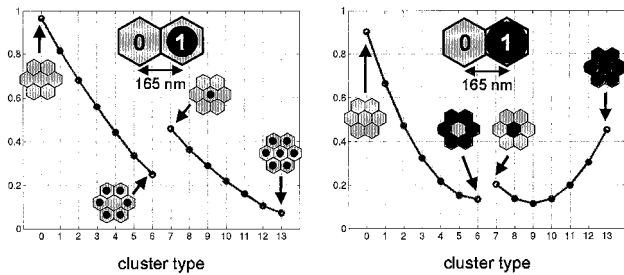


Fig. 6. Signal patterns for a 2D hexagonal bit lattice (drawn as a function of the cluster type) for  $\lambda = 405$  nm and NA of 0.85 with lattice parameter  $a_H = 165$  nm and diameters of pit holes  $b_{ph} = 122.5$  nm (left) and  $b_{ph} = 165$  nm (right).

agonal cluster consists of a central bit at its center position and of six nearest-neighbor bits at the neighboring lattice positions. Because the (nominal) spot is circularly symmetric, it is necessary only to identify the central bit and the number of pit bits among the nearest-neighbor bits (neglecting only for the purpose of identification the extra level dispersion that is due to nonlinear effects). This results in a total of 14 unique signal levels, for which each of the signal levels is  $N_n$ -fold degenerate with  $N_n = \binom{6}{n}$  and  $n$  is the number of nearest-neighbor pit bits ( $n = \sum_{i=1}^6 u_i$ ). A first example of the 2D hexagonal format with a hexagonal lattice parameter  $a_H = 165$  nm is shown in Fig. 6 for two pit-hole diameters,  $b_{ph} = 122.5$  nm (50% filling of hexagonal bit cell) and  $b_{ph} = 165$  nm (which is the maximum size of circular nonoverlapping pit holes). For a broad spiral consisting of 11 bit rows and with a guard band 1 bit row wide, this lattice parameter yields a capacity of  $1.4\times$  that of the BD format. The levels are normalized to the all-land reflection level (which is set equal to 1). A second example with a hexagonal lattice parameter  $a_H = 138$  nm is shown in Fig. 7 for two pit-hole diameters,  $b_{ph} = 102.5$  nm (50% filling) and  $b_{ph} = 138$  nm (maximum size), corresponding to a capacity that is  $2.0\times$  that of the BD format.

In these figures, level identification is based only on the six nearest-neighbor lattice bits (the so-called first shell), which make the most significant contribution to the 2D ISI. The scalar diffraction

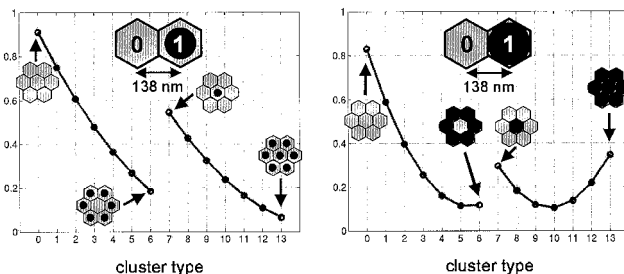


Fig. 7. Signal patterns for a 2D hexagonal bit lattice (drawn as a function of the cluster type) for  $\lambda = 405$  nm and NA of 0.85 with lattice parameter  $a_H = 138$  nm and diameters of the pit holes  $b_{ph} = 102.5$  nm (left) and  $b_{ph} = 138$  nm (right).

model, however, also takes all other relevant shells into account. The seven-bit hexagonal clusters are identified by a cluster index, computed as  $7u_0 + \sum_{i=1}^6 u_i$  (with the summation running over the six nearest neighbors). Signal-level variations that are due to differences in nonlinear effects within the seven-bit cluster and to the influence of the shells beyond the first shell are not shown. Instead, an average is taken across all possible bit patterns in these shells. This explains the fact that the signal level of the all-land cluster is not equal to 1, as we would expect from a normalized model, but somewhat smaller. Based on a detailed evaluation of the signal levels for various sizes of pit holes, and for a fixed phase depth of the pits  $\phi = 180^\circ$  (we omit the signal plots for the sake of brevity), it turns out that the best roll-off as a function of the number of neighboring pit bits  $n$  and maximum signal modulation are obtained for a pit hole that covers approximately half the area of the available hexagon. Indeed, for maximum signal modulation the signal level of the all-pit cluster should be as small as possible, which is to be expected for a 50% coverage criterion. The optimum pit-hole diameter  $b_{ph\ 50\%}$  equals

$$b_{ph\ 50\%} = \sqrt{\sqrt{3}/\pi} a_H. \quad (20)$$

Figures 6 and 7 reveal the quasi-linear roll-off of the signal levels for the 50% filling criterion (left); for the maximum (circular) pit-hole size (right), the signal folding becomes clear from the signal levels where the central bit of the cluster is a pit bit (1). The 50% filling criterion yields the best linearized channel condition. However, even in that case some obvious nonlinearities remain: (i) the signal range between minimum and maximum signal level is larger when the central bit of the cluster is a land bit (0; left-hand curve in each plot); (ii) each of the curves shows a nonlinear curvature, for a central bit that is both a land bit (0) and a pit bit (1), with the latter (right-hand curve in each plot) revealing the largest nonlinearity and the highest curvature. It can further be observed from Figs. 6 and 7 that the signal levels for bits 0 and bit 1 overlap. The range of signal overlap for the lower density of Fig. 6 amounts to three levels; for the higher density of Fig. 7 it amounts to somewhere from four to five levels. Although the signal overlap seems to be a serious problem at first sight, it is completely overcome in the signal processing of the digital receiver by means of a 2D maximum-likelihood bit detector.<sup>12,13</sup>

## 5. Reduction of Channel Parameters by Exploiting Rotational Symmetry in Two-Dimensional Optical Storage

A simplified but completely equivalent expression for the channel model of Eq. (14) or Eq. (17) in 2D optical storage can be obtained under the assumption of nominal read-out conditions with a nonaberrated rotationally symmetric spot profile.

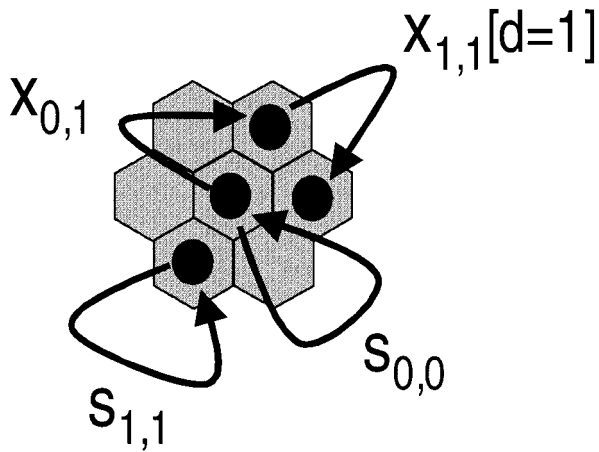


Fig. 8. Two types of bilinear interference of wave fronts on the seven-bit hexagonal cluster: self-interference  $s_{0,0}$  and  $s_{1,1}$ ; cross interference  $x_{0,1}$  and  $x_{1,1}(1)$ .

### A. General Case

The signal-processing model of Section 2 yields linear and bilinear terms. Among the bilinear terms we have self-interference terms for each pit bit (close enough to the center that the bit is within the area of the illuminating spot), and cross-interference terms for each pit pair (with both pit bits within the area of the illuminating spot). These two types of bilinear term are illustrated in Fig. 8. For the linear interferences, the only differentiating parameter is the distance from the current pit bit to the center of the spot (assumed to be centered on the central bit). It is therefore advantageous to classify the neighboring bits into shells (or rings), where all bits in a given shell have the same distance to the center of the spot. We distinguish shells with increasing distance  $d$  toward the center of the spot: shell 1 consists of the nearest neighbors of the central bit, all at distance  $d = 1$ ; shell 2 consists of the next-nearest neighbors of the central bit, all at  $d = \sqrt{3}$ ; shell 3 consists of the next-next-nearest neighbors of the central bit, all at  $d = \sqrt{4}$ , and so on. We denote the number of pit bits in shell  $j$ ,  $n_j$ ; and the total number of shells that we

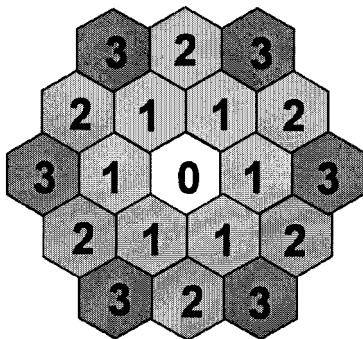


Fig. 9. Classification of neighboring bits (relative to the central bit at shell 0) in successive bit shells at distances equal to 1,  $\sqrt{3}$ , and  $\sqrt{4}$  for shells 1, 2, and 3, respectively (the shell numbers are indicated).

consider,  $N_{\text{shell}}$ . For  $N_{\text{shell}} = 3$ , all three shells are shown in Fig. 9.

The value of the coefficients for the kernels of the bilinear interferences depends in this simplified model on three parameters: (i) the distance of the first pit bit to the center of the spot, or, equivalently, its shell number  $i$ ; (ii) the distance of the second pit bit to the center of the spot, or, equivalently, its shell number  $j$ ; and (iii) the distance between the two pit bits.

When we account for a number  $N_{\text{shell}}$  of shells, signal waveform  $I$  can be modeled as a sum of five basic terms:

$$\begin{aligned}
 I = & 1 - 2[1 - \cos(\phi)]u_0(l_0 - s_{0,0}) \\
 & - 2[1 - \cos(\phi)] \sum_{j=1}^{N_{\text{shell}}} n_j(l_j - s_{j,j}) \\
 & + 4[1 - \cos(\phi)]u_0 \sum_{j=1}^{N_{\text{shell}}} n_j x_{0,j} \\
 & + 4[1 - \cos(\phi)] \sum_{j=1}^{N_{\text{shell}}} \sum_{i \geq j}^{N_{\text{shell}}} \sum_{d \in D_{i,j}} p_{i,j}(d) x_{i,j}(d).
 \end{aligned} \tag{21}$$

In Eq. (21) we have used the following notations:  $u_0$  is the unipolar bit value of the central bit, at which the laser spot is centered;  $n_j$  is the number of neighboring pit bits in shell  $j$ ;  $l_0$  is the tap value of the linear interference kernel for the central pit bit;  $l_j$  is the tap value of the linear interference kernel for a neighboring pit bit in shell  $j$ ;  $s_{0,0}$  is the value for self-interference of the central pit bit;  $s_{j,j}$  is the value for self-interference of a neighboring pit bit in shell  $j$ ;  $x_{0,j}$  is the value of the cross-interference kernel between the central pit bit and a neighboring pit bit in shell  $j$ ;  $D_{i,j}$  is the set of all possible nonzero distances  $d$  between a bit in shell  $i$  and a bit in shell  $j$ ;  $x_{i,j}(d)$  is the value of the cross-interference kernel between two neighboring pit bits, with one pit bit in shell  $i$ , the other pit bit in shell  $j$ , and a distance equal to  $d$ ; and finally,  $p_{i,j}(d)$  is the number of the last-named neighboring pit pairs.

Each of the five terms in Eq. (21) has a straightforward interpretation. The first term is a (normalized) constant term. The second term is the interference that results only from the central pit bit. The third term is a sum over all shells, with for each shell  $j$  the interference that results only from each individual pit bit in the shell. The fourth term is a sum over all shells, with for each shell  $j$  the cross interference of each pit bit in the shell with the central pit bit. And, finally, the fifth term in Eq. (21) is a double sum over all shells, with for each pair of shells  $i$  and  $j$  the cross interference of a pit bit in shell  $i$  and a pit bit in shell  $j$  at a distance  $d$ .

The sets  $D_{i,j}$  of distances  $d$  for  $N_{\text{shell}} = 3$  are  $D_{1,1} = \{1, \sqrt{3}, \sqrt{4}\}$ ,  $D_{1,2} = \{1, \sqrt{4}, \sqrt{7}\}$ ,  $D_{1,3} = \{1, \sqrt{3}, \sqrt{7}, \sqrt{9}\}$ ,  $D_{2,2} = \{\sqrt{3}, \sqrt{9}, \sqrt{12}\}$ ,  $D_{2,3} = \{1, \sqrt{7}, \sqrt{13}\}$ , and  $D_{3,3} = \{\sqrt{4}, \sqrt{12}, \sqrt{16}\}$  (all measured in units of  $a_H$ ).

**Table 1. Values of Nearest-Neighbor Bit Pairs [ $p_{1,1}(1)$ ] at Distance  $d = 1$**

Number of Nearest-Neighbor Bits $n_1$	Number of Neighboring Pit Pairs [ $p_{1,1}(1)$ ]	Average Value $\langle p_{1,1}(1) \rangle$
0	0	0
1	0	0
2	0, 1	0.4
3	0, 1, 2	1.2
4	2, 3	2.4
5	4	4
6	6	6

**B. Simplified Four-Parameter Model for Hexagonal Lattice Parameter  $a_H = 165$  nm**

A further approximating simplification of the multiple-shell rotationally symmetric channel model of Eq. (21) can be made when we limit all interferences to the first shell. A next approximating step is to neglect all cross interferences (between pit bits of shell 1) for pit bits that are separated by a distance larger than 1: In fact, we then consider only nearest-neighbor cross interference. Such an approximation turns out to be valid for the situation that the hexagonal lattice parameter equals  $a_H = 165$  nm (for a BD optical pickup unit). The signal waveform of Eq. (21) becomes in that case

$$\begin{aligned}
 I \approx & 1 - 2[1 - \cos(\phi)]u_0(l_0 - s_{0,0}) \\
 & - 2[1 - \cos(\phi)]n_1(l_1 - s_{1,1}) \\
 & + 4[1 - \cos(\phi)]u_0n_1x_{0,1} \\
 & + 4[1 - \cos(\phi)]p_{1,1}(1)x_{1,1}(1). \quad (22)
 \end{aligned}$$

This is essentially a four-parameter channel model. There is one global channel parameter for each of the four nontrivial terms in relation (22): ( $l_0 - s_{0,0}$ ) for the linear ISI of the central bit; ( $l_1 - s_{1,1}$ ) for the linear ISI of the nearest-neighbor bits;  $x_{0,1}$  for the nonlinear ISI between the central and the nearest-neighbor bits; and  $x_{1,1}(1)$  for the nonlinear ISI between nearest-neighbor bit pairs. Note that this simplified model needs only three parameters from the channel bit stream for each bit position: The central bit value  $u_0$ , the number of nearest-neighbor bits  $n_1$ , and the number of nearest-neighbor bit pairs at distance  $d = 1$ , denoted  $p_{1,1}(1)$ . The possible values of parameter  $p_{1,1}(1)$  (and its average value) are shown for all seven values of the number of nearest-neighbor pit bits  $n_1$  (of the first shell) in Table 1.

A simplified channel model with only a limited number of canonical channel parameters is ideal to serve as a compact nonlinear target response in a partial-response maximum-likelihood bit detector (see Ref. 18 for partial-response maximum-likelihood bit detection and target responses for linear 1D channel models).

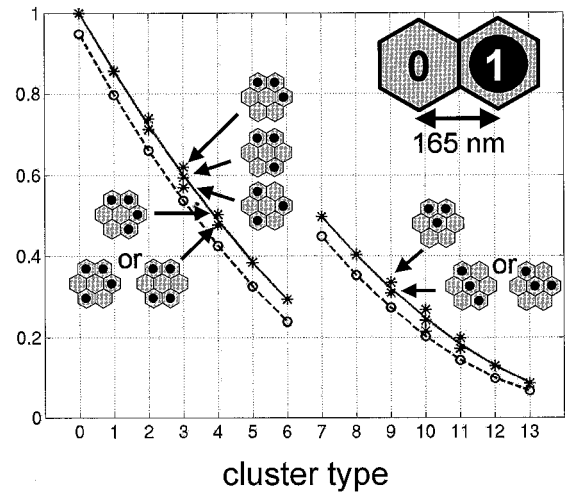


Fig. 10. Signal patterns (as a function of the cluster type) with lattice parameter  $a_H = 165$  nm and diameter of the pit hole  $b_{ph} = 122.5$  nm. The solid curves represent the average signal value for a four-parameter (single-shell) model, averaged for all possible clusters that have a fixed number of nearest neighbors. The stars represent different signal values, which depend on the number of two bit pairs of neighbor bits [denoted by the parameter  $p_{1,1}(1)$ ] for the four-parameter model. The dashed curves (with open circles) represent the averaged signal levels for the full model (with five shells).

**C. Simulation and Analysis of Main Nonlinearities for Hexagonal Lattice Parameter  $a_H = 165$  nm**

Figure 10 shows the signal pattern for  $a_H = 165$  nm and pit diameter  $b_{ph} = 122.5$  nm according to relation (22). From the figure we can clearly observe the two sets of eleven different signals as the isolated stars (one set for the central bit equal to 0; another set for the central bit equal to 1) according to the number of different  $p_{1,1}(1)$  parameters in Table 1. The average signal value (indicated by the solid curve in Fig. 10) is obtained as the average over all clusters with a given value of the number of nearest pit neighbors  $n_1$  (ranging from 0 to 6). This average value is determined by the value of  $\langle p_{1,1}(1) \rangle$  that is listed in the rightmost column of Table 1. Inasmuch as  $x_{1,1}(1)$  is a positive number, the graphs curve in an upward direction for higher values of  $n_1$  (for both cases,  $u_0 = 0$  and  $u_0 = 1$ ). Thus, in conclusion, there are two basic types of nonlinearity in this simplified model. First, there is the nonlinearity associated with cross interference  $x_{1,1}(1)$ , which is governed by the number of pit pairs  $p_{1,1}(1)$ . Second, there is the nonlinearity associated with cross interference  $x_{0,1}$ , which depends on the number of pit pairs that contain the central pit bit and one of the pit bits among the nearest neighbors of the central bit (the number of which is defined as  $n_1$ ): So the prefactor of  $x_{0,1}$  equals  $u_0n_1$  (thus linear in  $n_1$ , and nonzero only when  $u_0 = 1$ ). Because  $x_{0,1}$  is a positive number, the second type of nonlinearity boils down to a less negative slope of the linear interferences when the central bit is  $u_0 = 1$ , compared with  $u_0 = 0$ .

In addition, Fig. 10 also shows the signal levels for

the full model, i.e., with five shells included (dashed curves). The curve for the four-parameter model shows an offset relative to the full-model curve, but the overall shapes of the two curves are almost identical. The offset is caused by interferences that involve pit bits beyond the first shell of neighbors. Further note that the offset depends slightly on the cluster type because of nonlinear effects: The smallest offset between the four-parameter model and the full-model curves occurs at the all-pit cluster (with index 13).

## 6. Conclusions and Subjects for Future Study

A new, computationally efficient channel model for read-out of optical disks based on scalar diffraction has been derived. The new model does not require additional approximations on top of the basic assumption of scalar diffraction. The model is convenient from a signal-processing point of view because it is written in closed-form with explicit dependence on the channel bits that are written to the disk; the model comprises kernels for linear and nonlinear interferences. The model has been applied for 1D and 2D optical storage. For 2D optical storage, for which the bits are arranged on a 2D hexagonal lattice, we have addressed the issue of signal folding, which is due to severe channel nonlinearities: One can linearize the overall channel to a satisfactory level by assigning to each pit bit a pit mark that covers not more than 50% of the bit cell. The new signal-processing model has yielded additional insights into the origin of the nonlinearities of the signal waveform. Finally, for 2D optical storage we have also described signal modeling schemes with a reduced number of channel parameters by making use of the rotational symmetry of the laser spot for read-out under nominal nonaberrated conditions.

As subjects for potential future study we identify a couple of extensions of the current channel model. A first extension is concerned with 1D optical storage and the practical situation in which pit marks are systematically too large (too small), thereby reflecting, e.g., for a read-only disk the overetching (underetching) conditions during manufacture of the stamper disk. This phenomenon can be modeled in terms of a nonlinear disk reflection function  $r(\mathbf{R})$ : the nonlinear term is triggered at the edges of a contiguous pit mark and provides for the expansion or compression of the pit window at the pit bits that are located at the edges of the pit mark. Note that, with the disk reflection function having terms of maximum second order in the channel bits, the signal waveform will contain terms up to fourth order in the channel bits. A second extension of our model is concerned with a multichannel situation achieved through partitioning of the photodetector (each partition corresponds to one channel). The approach followed in this paper can be applied for each of these channels separately, yielding a signal waveform that is expressed in linear and nonlinear interference with kernels that are characteristic for the channel at hand. Such an approach can be applied for detector

partitioning in the plane of the exit pupil as well as for detector partitioning in the image plane, e.g., the image plane of an additional astigmatic lens with a quadrant detector as is typically used for an astigmatic focus servo system. Yet another possible extension of the model of this paper is concerned with 1D or 2D optical storage by use of multilevel instead of binary modulation and in which pit hole sizes may vary to generate the required multilevel signal amplitudes.

This research is part of a European IST (Information Science Technologies) project called "TwoDOS" (project IST-2001-34168). The author acknowledges the valuable contributions of all project members [Philips Research, University of Limerick, Eindhoven University of Technology, University of Lancaster, Philips ODT (Optical Disk Technology Center), and HW Communications] to this research. In addition, the author acknowledges stimulating discussions with Bob van Someren and Bin Yin (both of Philips Research).

## References

1. J. Pasman, "Vector theory of diffraction," in *Principles of Optical Disc Systems*, E. R. Pike, ed. (Adam Hilger, Bristol, UK, 1985), Chap. 3, pp. 88–124.
2. J. M. Brok and H. P. Urbach, "Simulation of polarization effects in diffraction problems of optical recording," *J. Mod. Opt.* **49**, 1811–1829 (2002).
3. H. H. Hopkins, "Diffraction theory of laser read-out systems for optical video discs," *J. Opt. Soc. Am.* **69**, 4–24 (1979).
4. J. Braat, "Read-out of optical discs," in *Principles of Optical Disc Systems*, E. R. Pike, ed. (Adam Hilger, Bristol, UK, 1985), Chap. 2, pp. 7–87.
5. J. W. Goodman, *Introduction to Fourier Optics*, 2nd ed. (McGraw Hill, New York, 1996).
6. "120 mm DVD-Read-Only Disk," 3rd ed., ECAM Standard 267 (April 2001), [www.ecma.ch](http://www.ecma.ch).
7. S. Kobayashi, "Nonlinear model for an optical read-only-memory disk readout channel based on an edge-spread function," *Appl. Opt.* **41**, 2679–2685 (2002).
8. H. Pozidis, J. W. M. Bergmans, and W. M. J. Coene, "Modeling and compensation of asymmetry in optical recording," *IEEE Trans. Commun.* **50**, 2052–2063 (2002).
9. T. D. Milster, "New way to describe diffraction from optical disks," *Appl. Opt.* **37**, 6878–6883 (1998).
10. P. W. Nutter and C. D. Wright, "A new technique for the prediction and correction of nonlinearities in simulated optical readout waveforms," in *Optical Data Storage 2001*, T. Hurst and S. Kobayashi, eds., *Proc. SPIE* **4342**, 82–84 (2002).
11. P. A. M. Dirac, *The Principles of Quantum Mechanics*, 4th ed. (Clarendon, Oxford, 1981).
12. W. M. J. Coene, "Two-dimensional optical storage," in *Optical Data Storage 2003*, M. O'Neill and N. Miyagawa, eds., *Proc. SPIE* **5069**, 90–92 (2003).
13. A. H. J. Immink, W. M. J. Coene, A. M. van der Lee, C. Busch, A. P. Hekstra, J. W. M. Bergmans, J. Riani, S. J. L. van Beneden, and T. Conway, "Signal processing and coding for two-dimensional optical storage," in *GLOBECOM 2003—2003 IEEE Global Telecommunications Conference* (IEEE, Piscataway, New Jersey, to be published).
14. T. Narahara, S. Kobayashi, M. Hattori, Y. Shimpuku, G. van den Enden, J. Kahlman, M. van Dijk, and R. van Woudenberg, "Optical disc system for digital video recording," *Jpn. J. Appl. Phys. Part 1* **39**, 912–919 (2002).

15. B. Stek, R. Otte, T. Jansen, and D. Modrie, "Advanced signal-processing for the Bluray disc system," in *Joint International Symposium on Optical Memory and Optical Data Storage ISOM/ODS 2002* (IEEE/LEOS, Piscataway, New Jersey, 2002), pp. 263–265.
16. W. Weeks and R. E. Blahut, "The capacity and coding gain of certain checkerboard codes," *IEEE Trans. Inf. Theory* **44**, 1193–1203 (1998).
17. T. Kato, S. Taira, T. Maeda, Y. Katayama, and T. Nishiya, "Two-dimensional run-length-limited code and partial response maximum likelihood system with multi-track recording," in *Joint International Symposium on Optical Memory and Optical Data Storage ISOM/ODS 2002* (IEEE/LEOS, Piscataway, New Jersey, 2002), pp. 51–53.
18. J. W. M. Bergmans, *Digital Baseband Transmission and Recording* (Kluwer Academic, Dordrecht, The Netherlands, 1996).